

Axisymmetrical free-vibration analysis of liquid-storage tanks considering the liquid compressibility

Jin-Rae Cho[†] and Jin-Kyu Lee[‡]

School of Mechanical Engineering, Pusan National University, Pusan 609-735, Korea

Abstract. In this paper, we address the numerical investigation on the effect of liquid compressibility onto the natural frequency of liquid-filled containers. Traditionally the liquid motion has been treated as an ideal fluid motion. However, from the numerical experiments for the axisymmetrical free-vibration of cylindrical liquid-storage tanks, we found that the relative difference in natural frequencies between ideal and compressible motions becomes remarkable, as the slenderness of tank or the relative liquid-fill height becomes larger. Therefore, in such cases of dynamic systems, the liquid compressibility becomes an important parameter, for the accurate vibration analysis. For the free-vibration analysis of compressible liquid-structure interaction we employed the coupled finite element formulation expressed in terms of the acoustic wave pressure and the structure deformation.

Key words: axisymmetrical free vibration; liquid compressibility; acoustic wave; coupled liquid-structure formulation; relative difference; parametric variation.

1. Introduction

In the free vibration and seismic response analysis of liquid-structure interaction problems, the formulation of hydrodynamic pressure field in liquid plays an important role. Traditionally, the liquid motion in stationary engineering liquid-storage tanks has been regarded as an ideal fluid flow, according to its relatively lower frequency and simpler flow behavior. As a result, the liquid motion is governed by Laplace equation in terms of a velocity potential function, as well the hydrodynamic pressure field by a similar one resulted from combining the continuity and Euler momentum equations.

Housner (1957) and other early investigators laid down a fundamental theoretical framework for ideal-liquid-structure interaction problems. Besides an ideal flow assumption, early studies involved further simplifications, the exclusion of the container flexibility and the liquid free-surface sloshing. Since Veletsos (1963) emphasized first the importance of the former, the refinement and assessment of the early studies, by reflecting the container flexibility, have been widely performed. On the other hand, the influence of the latter was investigated first by Abramson (1966) and Moiseev and Rumyantsev (1968). Both effects influence the free vibration behavior as well as the seismic response, however the influence intensity has been numerically found to be negligible (Cho *et al.* 2000, Haroun and Tayel 1985). Literature and the extensive work on numerical formulation

[†] Associate Professor

[‡] Graduate Student

considering sloshing effect may refer to a book by Morand and Ohayon (1995).

The viscosity effect of real liquids, while assumed to be ideal, is modeled by means of a damping term, by measuring from experiments, that is introduced in the dynamic motion of the container. In fact, the viscosity does not influence the free vibration behavior itself of real liquid-storage tanks (Conca *et al.* 1997). But, the consideration of real viscous liquid leads to the complex situation in the formulation of hydrodynamic pressure field. As for the compressibility, Walker (1980) introduced a boundary element formulation considering its effect, and reported that it should be regarded for the liquid-structure interactions under high frequency excitations. The research literature for recent studies on fluid-structure interactions is well summarized in a paper by Mackerle (1999).

In a series of our previous works (Cho *et al.* 1999, 2000, 2001a and 2001b) for ideal-liquid-storage tanks, we in this paper intend to quantitatively and numerically investigate the effect of liquid compressibility upon the free vibration behavior. For this goal, we establish a finite element formulation and develop a test finite element program. Through the comparative numerical experiments, we examine the relative difference in natural frequencies between compressible and incompressible liquid motions.

2. Compressible liquid-structure interaction problems

We consider the axisymmetric free-vibration behavior of cylindrical tank of uniform thickness h , as shown in Fig. 1, in which irrotational inviscid compressible liquid is filled up to the height H^L and the bottom plate is fixed to ground. The superscripts L and S in symbols refer to liquid and structure, respectively, throughout this paper. And we denote the liquid velocity vector by $\mathbf{v} = \{v_r, v_z\}^T$ while the structure dynamic displacement by $\mathbf{u} = \{u_r, u_z\}^T$, respectively.

2.1 Pressure field in compressible liquid region

In the liquid motion within storage tanks, the mean flow and dissipation are absent so that $\nabla \cdot \mathbf{v} =$

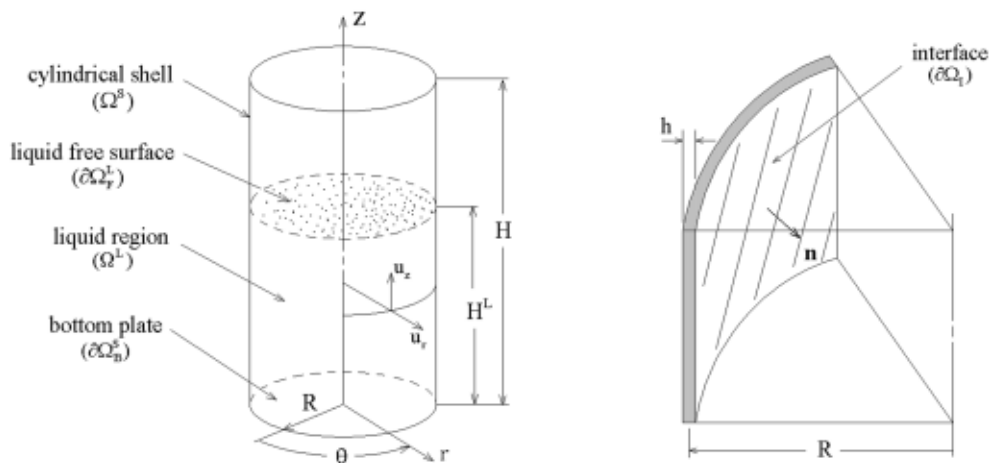


Fig. 1 Geometry and symbol definition of compressible liquid-storage tank

$\frac{1}{r} \frac{\partial}{\partial r}(rv_r) + \frac{\partial v_z}{\partial z} = 0$, further the acoustic amplitude caused by the fluctuation of pressure (i.e., acoustic pressure $p_c(r, z; t)$) is usually small relative to the mean pressure $p_o(r, z; t)$ (Howe 1998). Then, for irrotational inviscid compressible flows, combining the continuity equation and the Navier-Stokes equations leads to the well-known wave propagation equation in terms of dynamic pressure $p(r, z; t) = p_o + p_c$:

$$\frac{1}{c^2} \frac{\partial^2 p}{\partial t^2} - \nabla^2 p = 0, \quad \text{in } \Omega_L \tag{1}$$

together with corresponding boundary conditions

$$\nabla p \cdot \mathbf{n} = \left\{ \begin{array}{l} -\rho_o^L \mathbf{n} \cdot \frac{\partial^2 \mathbf{u}}{\partial t^2}, \quad \text{on } \partial\Omega_I \\ 0, \quad \text{on } \partial\Omega_B^L \\ p=0, \quad \text{on } \partial\Omega_F^L \end{array} \right\} \tag{2}$$

where ∇ and ∇^2 are gradient and Laplace operators defined in axisymmetric cylindrical coordinates. The speed of sound c in Eq. (1) is defined by $\sqrt{k/\rho_o^L}$, in which k and ρ_o^L denote respectively the bulk modulus and the mean density of liquid. The compatibility condition between normal pressure and acceleration of structure deformation field $\mathbf{u}(r, z; t)$ is specified on the liquid-structure interface $\partial\Omega_I$. By specifying the boundary condition on the liquid free surface $\partial\Omega_F^L$ as in Eq. (2), we exclude the free-surface sloshing effect of liquid. When it is included, the modal analysis becomes a nonlinear eigenvalue problem (Morand and Ohayon 1995, Cho *et al.* 2000).

Above pressure formulation can be easily switched to an alternative formulation in terms of compressible velocity potential $\varphi(r, z; t)$: $\mathbf{v} = \nabla \varphi$:

$$\nabla^2 \varphi - \frac{1}{c^2} \frac{\partial^2 \varphi}{\partial t^2} = 0, \quad \text{in } \Omega^L \tag{3}$$

equipped with

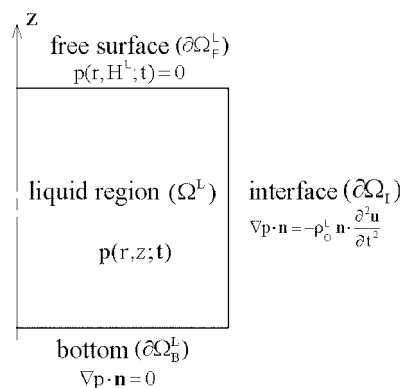


Fig. 2 Boundary conditions specified for the axisymmetric liquid region

$$\nabla \varphi \cdot \mathbf{n} = \begin{cases} \frac{\partial u_r}{\partial t}, & \text{on } \partial\Omega_I \\ 0, & \text{on } \partial\Omega_F^L \text{ and } \partial\Omega_B^L \end{cases} \quad (4)$$

For harmonically oscillating dynamic pressure described by

$$p = \bar{p}(\mathbf{x}) e^{i\omega t} \quad (5)$$

the above wave equation reduces to the Helmholtz equation:

$$\frac{\omega^2}{c^2} p + \nabla^2 p = 0 \quad (6)$$

2.2 Dynamic displacement field in structure region

Viewing liquid-storage container as a three-dimensional axisymmetric linear elastic structure, as opposed to usual shells, we have the dynamic motions given by

$$\left. \begin{aligned} \frac{\partial \sigma_{rr}}{\partial r} + \frac{\partial \sigma_{zr}}{\partial z} + \frac{\sigma_{rr} - \sigma_{\theta\theta}}{r} - \rho^s \frac{\partial^2 u_r}{\partial t^2} &= 0 \\ \frac{1}{r} \frac{\partial}{\partial r} (r \sigma_{rz}) + \frac{\partial \sigma_{rz}}{\partial z} - \rho^s \frac{\partial^2 u_z}{\partial t^2} &= 0 \end{aligned} \right\}, \text{ in } \Omega^s \quad (7)$$

equipped with

$$\left. \begin{aligned} \sigma_{ij} n_j &= -p n_i, & \text{on } \partial\Omega_I \\ u_i &= 0, & \text{on } \partial\Omega_B^s \end{aligned} \right\} \quad (8)$$

where i and j refer to r and z . In addition, σ_{ij} denote stress components corresponding to Cauchy strains given by

$$\begin{Bmatrix} \epsilon_{rr} \\ \epsilon_{\theta\theta} \\ \epsilon_{zz} \\ \epsilon_{rz} \end{Bmatrix} = \begin{bmatrix} \partial/\partial r & 0 \\ 1/r & 0 \\ 0 & \partial/\partial z \\ \partial/2\partial z & \partial/2\partial r \end{bmatrix} \begin{Bmatrix} u_r \\ u_z \end{Bmatrix} = [\mathbf{D}] \begin{Bmatrix} u_r \\ u_z \end{Bmatrix} \quad (9)$$

In order for the modal analysis, by separating structure and liquid regions, the hydrodynamic interference on $\partial\Omega_I$ should be transformed into equivalent mass added to the counterpart. For ideal- fluid-structure interactions, the numerical procedure becomes linear (Appa Rao *et al.* 1993) when the liquid free-surface sloshing excludes, otherwise it becomes frequency-dependent nonlinear, as mentioned before. For the nonlinear case, one needs a sort of predictor-corrector-type numerical iteration scheme, as one proposed by authors (Cho, Song and Lee 2001) for separate modal analysis including the ideal liquid free-surface sloshing. This nonlinearity occurs also when one tries to analyze compressible-liquid-structure interactions according to the separate modal analysis, even

when the liquid free-surface sloshing is not included. The reader, from Eq. (6) and the interface boundary condition in Eq. (8), can easily realize that the hydrodynamic pressure acting on $\partial\Omega_I$ becomes frequency-dependent.

3. Coupled finite element approximations

According to usual variational formulation, together with defining the space $V(\Omega^L)$ of admissible pressure field given by

$$V(\Omega^L) = \{q: q \in H^1(\Omega^L) | q=0 \text{ on } \partial\Omega_F^L\} \tag{10}$$

the wave equation in Section 2.1 results in: Find $p \in V(\Omega^L)$ such that, $\forall q \in V(\Omega^L)$

$$\int_{\Omega^L} \left[\frac{1}{c^2} q \frac{\partial^2 p}{\partial t^2} + \nabla q \cdot \nabla p \right] dr dz = \int_{\partial\Omega_I} -q \left(\rho_0^L \mathbf{n} \cdot \frac{\partial^2 \mathbf{u}}{\partial t^2} \right) dz \tag{11}$$

Using two-dimensional isoparametric finite-element basis functions, we approximate trial and test pressure fields and structure deformation

$$p^h = \Phi \bar{p}, \quad \mathbf{u}^h = \Psi \bar{\mathbf{u}}, \quad q^h = \Phi \bar{q} \tag{12}$$

where Φ is the $(1 \times N)$ basis-function matrix and Ψ the $(2 \times 2M)$ basis function matrix.

Substituting finite element approximations into the variational form (11), we obtain

$$[\mathbf{M}^L] \{ \ddot{\bar{p}} \} + [\mathbf{K}^L] \{ \bar{p} \} = -\rho_0^L [\mathbf{R}^L] [\mathbf{S}] \{ \ddot{\bar{\mathbf{u}}} \} |_{\partial\Omega_I} \tag{13}$$

with matrices defined by

$$[\mathbf{M}^L] = \frac{1}{c^2} \int_{\Omega^L} \Phi^T \Phi dr dz \tag{14}$$

$$[\mathbf{K}^L] = \int_{\Omega^L} (\nabla \Phi)^T (\nabla \Phi) dr dz \tag{15}$$

$$[\mathbf{S}] = \int_{\partial\Omega_I} \Phi^T (\{ \mathbf{n} \} \Psi) dz \tag{16}$$

where $\{ \mathbf{n} \}$ is defined as $\{ n_r, n_z \}$. In Eq. (13), $\{ \bar{\mathbf{u}} \} |_{\partial\Omega_I}$ indicates the structure nodal vector restricted on the liquid-structure interface with M^I nodes, thus its size is $(2M^I \times 1, M^I < N)$. While $[\mathbf{S}]$ is of $(M^I \times 2M^I)$ size and $[\mathbf{R}^L]$ is the $(N \times M^I)$ row extension operator defined by

$$[R_{ij}^L] = \begin{cases} 1, & [\mathbf{M}^L]_{i-row}^{Node\ No.} = [\mathbf{S}]_{j-row}^{Node\ No.} \\ 0, & \text{otherwise} \end{cases} \tag{17}$$

This row extension operator, while most of its components are 0, relocates rows of $[\mathbf{S}]$ into the correct row positions based on the two matrices in Eq. (13).

Defining the space $W(\Omega^S)$ of admissible double-vector dynamic displacement field, for the container, by

$$W(\Omega^s) = \{\mathbf{v}: \mathbf{v} \in [H^1(\Omega^s)]^2 | \mathbf{v} = \mathbf{0} \text{ on } \partial\Omega_B^s\} \quad (18)$$

variational formulation of the dynamic motion is as follows: Find $\mathbf{u} \in W(\Omega^s)$ such that, $\forall \mathbf{v} \in W(\Omega^s)$

$$\int_{\Omega^s} \left[\varepsilon_{ij}(\mathbf{v}) \sigma_{ij}(\mathbf{u}) + \varepsilon_{\theta\theta}(\mathbf{v}) \sigma_{\theta\theta}(\mathbf{u}) + \rho^s v_i \frac{\partial^2 u_i}{\partial t^2} \right] dr dz = \int_{\partial\Omega_l} p n_i v_i dr dz \quad (19)$$

According to finite element approximations for the dynamic displacement and the pressure field given in Eq. (12), we arrive at

$$[\mathbf{M}^S] \{\ddot{\bar{\mathbf{u}}}\} + [\mathbf{K}^S] \{\bar{\mathbf{u}}\} = [\mathbf{R}^S] [\mathbf{S}^T] \{\bar{\mathbf{p}}\} |_{\partial\Omega_l} \quad (20)$$

with matrices:

$$[\mathbf{M}^S] = \int_{\Omega^s} \rho^s \Psi^T \Psi dr dz \quad (21)$$

$$[\mathbf{K}^S] = \int_{\Omega^s} (\mathbf{D}\Psi)^T \mathbf{E} (\mathbf{D}\Psi) dr dz \quad (22)$$

$$[\mathbf{S}^T] = \int_{\partial\Omega_l} (\{\mathbf{n}\} \Psi)^T \Phi dz \quad (23)$$

In Eq. (20), $\{\bar{\mathbf{p}}\} |_{\partial\Omega_l}$ is the $(M^l \times 1)$ pressure nodal vector restricted on $\partial\Omega_l$, and $[\mathbf{R}^S]$ the $(2M \times 2M^l)$ row extension operator, defined as similar as $[\mathbf{R}^L]$, which relocates rows of $[\mathbf{S}^T]$ into the correct row positions based on the two matrices in Eq. (20). In addition, in Eq. (22), \mathbf{E} is the material matrix consisting of Lamé constants that constitutes stresses and strains.

In order to couple two sets of matrix Eqs. (13) and (20), we need to extend the two restricted nodal vectors $\{\bar{\mathbf{u}}\} |_{\partial\Omega_l}$ and $\{\bar{\mathbf{p}}\} |_{\partial\Omega_l}$ to entire nodal vectors $\{\bar{\mathbf{u}}\}$ of structure and $\{\bar{\mathbf{p}}\}$ of liquid, respectively. So, using the two restriction operators, we have

$$\{\bar{\mathbf{u}}\} |_{\partial\Omega_l} = [\mathbf{R}^{S^T}] \{\bar{\mathbf{u}}\} \quad (24)$$

$$\{\bar{\mathbf{p}}\} |_{\partial\Omega_l} = [\mathbf{R}^{L^T}] \{\bar{\mathbf{p}}\} \quad (25)$$

Introducing these two relations into Eqs. (13) and (20), respectively, we obtain a coupled compressible-liquid-structure formulation:

$$\begin{bmatrix} \mathbf{M}^S & \mathbf{0} \\ \rho_0^L \mathbf{Q}^T & \mathbf{M}^L \end{bmatrix} \begin{Bmatrix} \ddot{\bar{\mathbf{u}}} \\ \ddot{\bar{\mathbf{p}}} \end{Bmatrix} + \begin{bmatrix} \mathbf{K}^S & -\mathbf{Q} \\ \mathbf{0} & \mathbf{K}^L \end{bmatrix} \begin{Bmatrix} \bar{\mathbf{u}} \\ \bar{\mathbf{p}} \end{Bmatrix} = \begin{Bmatrix} \mathbf{0} \\ \mathbf{0} \end{Bmatrix} \quad (26)$$

where

$$[\mathbf{Q}] = [\mathbf{R}^S] [\mathbf{S}^T] [\mathbf{R}^{L^T}] \quad (27)$$

In order to apply the standard eigenvalue computation methods, we symmetrize the equation system (26) according to a simple method suggested by Morand and Ohayon (1995). For harmonic

motions $\{\bar{\mathbf{u}}, \bar{\mathbf{p}}\}^T = \{\tilde{\mathbf{u}}, \tilde{\mathbf{p}}\}^T \cdot e^{i\omega t}$ together with introducing an additional variable $\tilde{\mathbf{q}}$ satisfying $\tilde{\mathbf{p}} = \omega^2 \tilde{\mathbf{q}}$, we easily rewrite Eq. (26) as

$$\left. \begin{aligned} (\mathbf{K}^S - \omega^2 \mathbf{M}^S) \tilde{\mathbf{u}} - \omega^2 \mathbf{Q} \tilde{\mathbf{q}} &= \mathbf{0} \\ \mathbf{M}^L (\tilde{\mathbf{p}} - \omega^2 \tilde{\mathbf{q}}) / \rho_0^L &= \mathbf{0} \\ \omega^2 [\mathbf{Q}^T \tilde{\mathbf{u}} + (\mathbf{M}^L \tilde{\mathbf{p}} - \mathbf{K}^L \tilde{\mathbf{q}}) / \rho_0^L] &= \mathbf{0} \end{aligned} \right\} \quad (28)$$

According to static condensation, we have

$$\tilde{\mathbf{q}} = (\mathbf{K}^L)^{-1} (\mathbf{M}^L \tilde{\mathbf{p}} + \rho_0^L \mathbf{Q}^T \tilde{\mathbf{u}}) \quad (29)$$

and

$$\left\{ \begin{bmatrix} \mathbf{K}^S & \mathbf{0} \\ \mathbf{0} & \mathbf{M}^L / \rho_0^L \end{bmatrix} - \omega^2 \begin{bmatrix} [\mathbf{M}^S + \rho_0^L \mathbf{Q} (\mathbf{K}^L)^{-1} \mathbf{Q}^T] & [\mathbf{Q} (\mathbf{K}^L)^{-1} \mathbf{M}^L] \\ [\mathbf{Q} (\mathbf{K}^L)^{-1} \mathbf{M}^L]^T & [\mathbf{M}^L (\mathbf{K}^L)^{-1} \mathbf{M}^L] / \rho_0^L \end{bmatrix} \right\} \begin{Bmatrix} \tilde{\mathbf{u}} \\ \tilde{\mathbf{p}} \end{Bmatrix} = \begin{Bmatrix} \mathbf{0} \\ \mathbf{0} \end{Bmatrix} \quad (30)$$

in which we use the symmetry of $[\mathbf{M}^L]$ and $[\mathbf{K}^L]$.

When liquid motion is assumed to be incompressible, $[\mathbf{M}^L]$ becomes identically a zero matrix (letting $1/c^2$ in Eq. (14) be zero). Then, above symmetric coupled equation system reduces to the separate free-vibration problem of structure containing incompressible liquid:

$$\{\mathbf{K}^S - \omega^2 [\mathbf{M}^S + \rho_0^L \mathbf{Q} (\mathbf{K}^L)^{-1} \mathbf{Q}^T]\} \tilde{\mathbf{u}} = \mathbf{0} \quad (31)$$

The term $[\rho_0^L \mathbf{Q} (\mathbf{K}^L)^{-1} \mathbf{Q}^T]$, the hydrodynamic effect by the mean pressure field, is defined as an added-mass matrix in incompressible-liquid-structure interactions (Cho *et al.* 2000).

From equation system (30) for compressible liquid motions, we realize that the hydrodynamic interference of liquid is divided into two, one by the mean pressure field p_o (i.e., the added mass of mean pressure (or one in incompressible case)) and the other by the acoustic wave pressure p_c (the terms including $[\mathbf{M}^L]$ matrix). It is worth to note, differing from the incompressible case, that the free-vibration can not be separately implemented when the liquid compressibility is considered.

4. Numerical experiments

According to the finite element formulation, we modified our test FEM program that has been previously developed for the free-vibration and seismic analysis of incompressible-liquid-storage tanks. In this test program, mesh generation and output visualization are implemented by utilizing pre- and post-processor modules of ANSYS commercial software.

In Table 1, we record geometry and material data of shell and liquid selected for the numerical experiments. In which the tank height and the liquid fill height are taken variable in order for the parametric investigation of the liquid compressibility.

Fig. 3(a) shows a finite element mesh generated with 8-node quadrilateral elements for the model tank with H/R of 2 and H^L/H of 1. In the radial direction, the liquid region is uniformly divided into

Table 1 Geometry and material data for numerical experiments

Items	Parameter	Data
Structure	Radius R (m)	20
	Height H (m)	Variable
	Thickness h (m)	0.0283
	Density ρ^s (kg/m ³)	7.85×10^3
	Young's modulus E (KPa)	21.5×10^7
	Poisson's ratio ν	0.3
Liquid	Fill height H^L (m)	Variable
	Mean density ρ_o^L (kg/m ³)	1,000
	Speed of sound c (m/s)	1,410

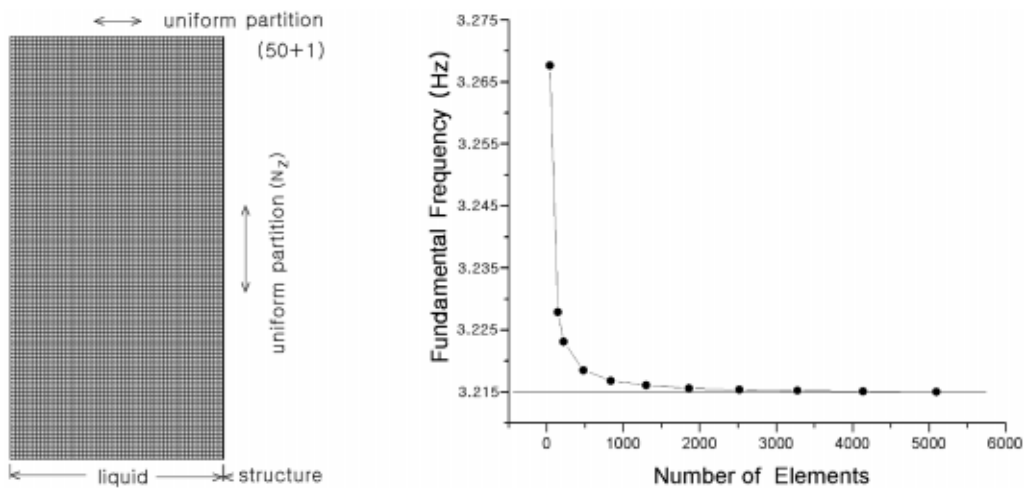


Fig. 3 Finite element mesh ($H/R=2$ and $H^L/H=1$) (a), and the variation of fundamental frequency to the element number (b)

fifty while the structure into one. On the other hand, we made uniform partition in the vertical direction N_z such that liquid elements become almost square. The variation of fundamental frequency to the element number for this mesh pattern is given in Fig. 3(b), from which we ensure that the assigned mesh density produces numerically high accuracy.

We carried out the comparative numerical experiments, in order to investigate the relative difference in natural frequencies between compressible and incompressible liquid motions, for various combinations of the relative tank height and the relative liquid fill height. The free-vibration analysis for the incompressible case was implemented with our previous test FEM program developed for the free-vibration and seismic analysis of incompressible-liquid-storage tanks. The computed numerical values are contained in Table 2. In order to retain the numerical error during iteration process through Lanczos transformation, we computed twenty natural frequencies for three lowest ones.

Fig. 4 presents the relative difference variations of fundamental frequencies, for three tank heights, with respect to the liquid fill height. By the relative difference is defined as $[(f^{incomp} - f^{comp})/$

Table 2 Comparison of natural frequencies for compressible- and incompressible-liquid-structure interactions for variable tank and liquid-fill heights

H/R	Mode	Compressible (Hz)					Incompressible (Hz)				
		Liquid-fill height H^L/H									
		0.2	0.4	0.6	0.8	1.0	0.2	0.4	0.6	0.8	1.0
2.0	1	14.44	7.85	5.32	4.01	3.22	15.06	8.34	5.69	4.30	3.45
	2	28.37	18.66	13.97	11.07	9.11	28.70	19.14	14.51	11.61	9.62
	3	33.18	25.18	19.78	16.34	13.88	33.24	25.53	20.22	16.84	14.41
1.0	1	24.10	14.47	10.24	7.86	6.36	24.59	15.07	10.81	8.35	6.78
	2	43.32	28.48	22.43	18.68	16.00	43.58	28.81	22.84	19.16	16.53
	3	64.66	37.09	29.59	25.20	22.13	64.87	37.33	29.89	25.55	22.53
0.5	1	37.87	23.73	17.92	14.39	11.96	38.21	24.20	18.48	14.98	12.55
	2	70.00	41.24	32.87	28.10	24.78	70.27	41.45	33.14	28.42	15.14
	3	83.57	54.82	42.03	36.04	32.11	83.57	55.01	42.21	36.26	32.36

$f^{comp}] \times 100\%$. First of all, we observe that the relative difference increases uniformly as either the relative tank height or the relative liquid fill height becomes larger. This reflects that the larger liquid amount becomes the higher acoustic wave influence is.

However, the relative-difference increase in proportion to the liquid-fill height becomes dull as the tank slenderness increases. This phenomenon is solely associated with the characteristic of equivalent liquid mass affecting the structure motion, i.e., added mass of liquid m^{add} , with respect to the slenderness of liquid H^L/R . Referring to the work of Cho *et al.* (1999) and Haroun (1983), the relative added mass to the total liquid mass m^{add}/m^{TOT} exhibits a saturation behavior along the liquid slenderness (refer to Fig. 5a). Since the relative added mass itself saturates in proportion to the increase of liquid slenderness H^L/R , the relative difference between compressible and incompressible liquid motions shows naturally the saturation behavior.

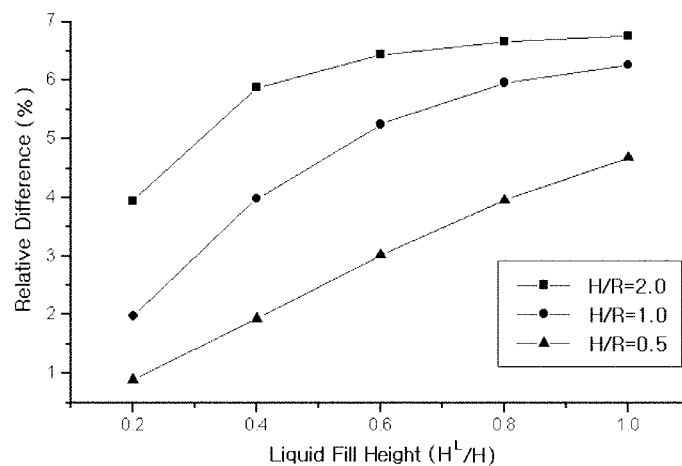


Fig. 4 Variations of the relative difference in fundamental frequencies, for different tank heights, to the liquid-fill height

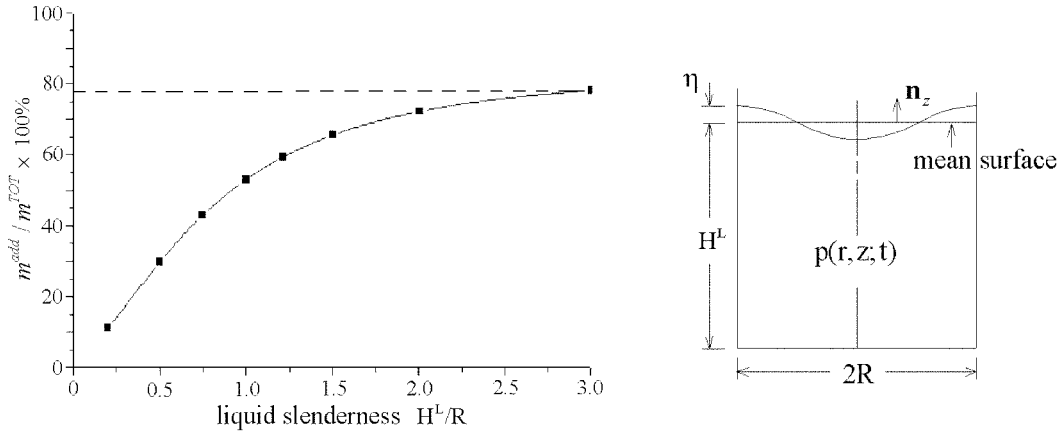


Fig. 5 Added mass saturation to the liquid slenderness (a), and the free-surface fluctuation (b)

Figs. 6-8 present the variations of relative difference in three lowest natural frequencies for three relative tank heights H/R of 2, 1 and 0.5, respectively. Similar to the fundamental frequency, the relative difference in second and third ones becomes larger as either the tank height or the liquid-fill height increases. However, from Fig. 6, we find that the saturation behavior occurred for the fundamental frequency, when the liquid slenderness becomes significantly larger, disappears as the natural frequency goes higher. Therefore, we conclude that the saturation behavior prevails as the natural frequency goes lower and the liquid slenderness H^L/R increases.

On the other hand, for each relative tank height the relative difference between compressible and incompressible liquid motions decreases uniformly in proportion to the increase of natural frequency. Referring to Fig. 5(b), the free-surface fluctuation η is $\nabla p \cdot \mathbf{n}_z / (\rho^L \omega^2)$ (Howe 1998). And this fluctuation height decreases uniformly as the natural frequency goes higher. Therefore, we can physically infer that the spatial variation of dynamic-pressure field diminishes in proportion to the natural frequency increase.

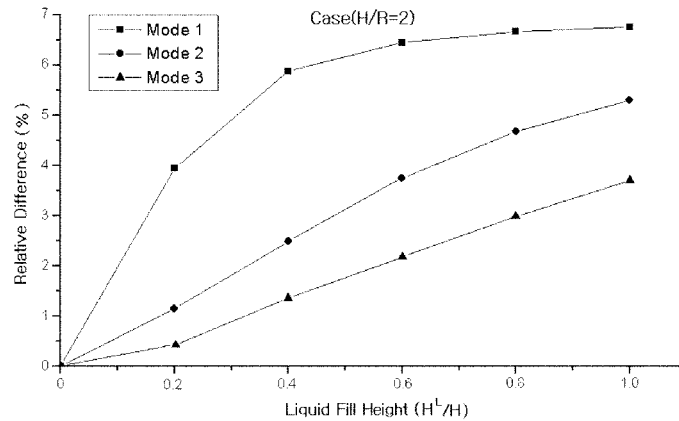


Fig. 6 Variations of the relative difference in three lowest natural frequencies when H/R is 2

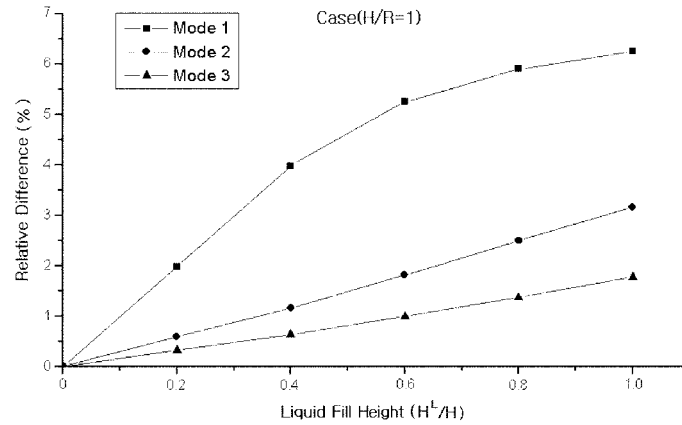


Fig. 7 Variations of the relative difference in three lowest natural frequencies when H/R is 1

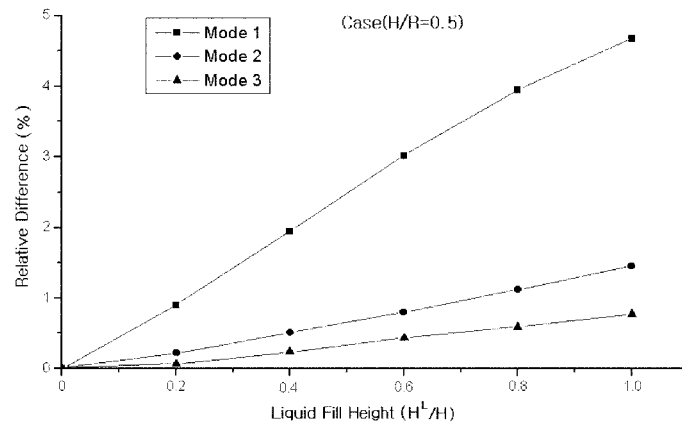


Fig. 8 Variations of the relative difference in three lowest natural frequencies when H/R is 0.5

Last three figures show the comparison of mode shapes and dynamic-pressure distributions, for three lowest natural frequencies, when H/R and H^L/H are respectively 3 and 1. In plots, displacement amplitudes and minimum/maximum dynamic pressure values are mass-matrix normalized. Since the compressible case includes an additional mass contribution $[M^L]$ due to the acoustic pressure field, as represented in Eqs. (26) and (30), it leads to smaller normalized values compared to the incompressible case.

We can not notice any remarkable difference, except for the difference in normalized amplitude values, in mode shapes between compressible and incompressible cases. But, we observe the noticeable difference in dynamic-pressure contours between both cases by minutely comparing the contour extension lengths in the radial direction. The compressible case shows smaller dynamic-pressure gradient, a little bit, in the radial direction, particularly near the vertical locations where mode shapes show convex and concave apices.

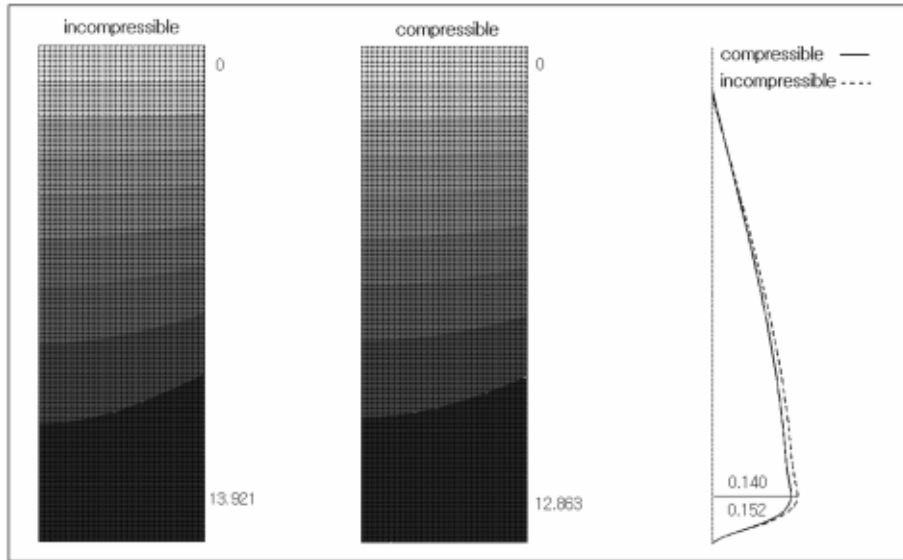


Fig. 9 Comparison of first mode shapes ($\times 10^{-6}$) and corresponding dynamic-pressure distributions (mass-normalized; $H/R=3$ and $H^L/H=1$)

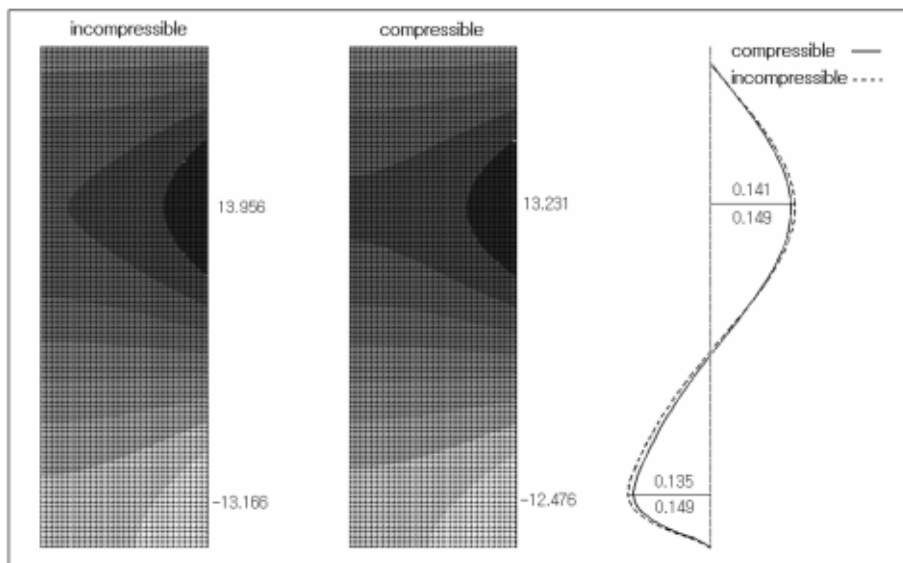


Fig. 10 Comparison of second mode shapes ($\times 10^{-6}$) and corresponding dynamic-pressure distributions (mass-normalized; $H/R=3$ and $H^L/H=1$)

5. Conclusions

In order to investigate the effect of liquid compressibility on the free-vibration of stationary liquid-storage tanks, we numerically studied the axisymmetrical free-vibration of cylindrical liquid-

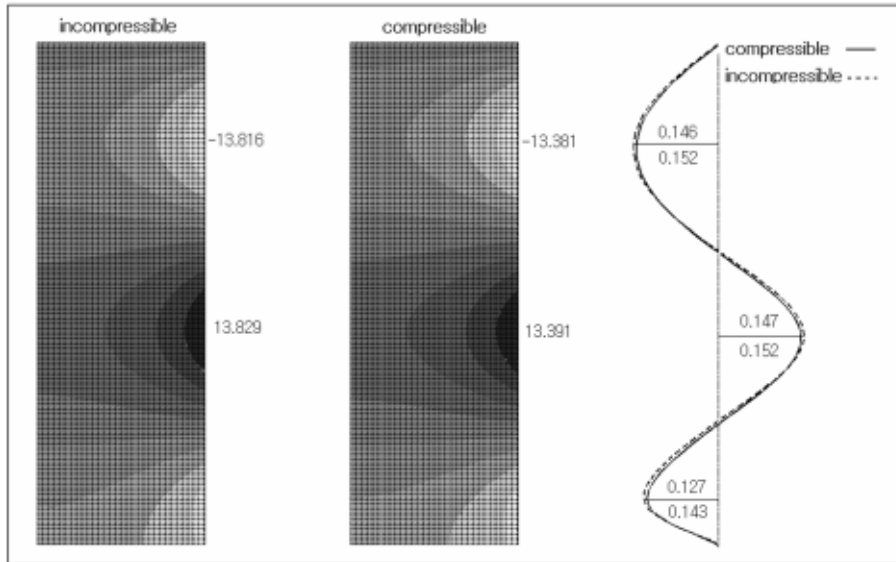


Fig. 11 Comparison of third mode shapes ($\times 10^{-6}$) and corresponding dynamic-pressure distributions (mass-normalized; $H/R=3$ and $H^L/H=1$)

storage tank. This is because, among free-vibration modes, the axisymmetrical mode is more associated with the liquid compression.

For this goal, we established a coupled finite element formulation, and developed a test FEM program by modifying our previous one that was developed for the free-vibration and seismic analysis of incompressible-liquid-storage tanks. With the test program, we carried out the comparative numerical experiments, in order to examine the difference in natural frequencies between compressible and incompressible liquid motions, for various relative tank and liquid fill heights.

From the numerical results, we observed that the relative difference increases as either the relative tank height or the relative liquid fill height becomes larger. As well as, it decreases in proportion to the increase of natural frequency. On the other hand, we observed noticeable difference in mass-normalized dynamic pressure distributions, even though any remarkable difference in mode shapes except for the difference in normalized amplitudes is not shown.

Acknowledgements

The authors gratefully acknowledge the financial support for this work by Korea Science and Engineering Foundation under Grant No. 981-1002-016-2 and Agency for Defense Development under Contract No. ADD-00-5-6.

References

Abramson, H.N. (1966), *The Dynamic Behavior of Liquids in Moving Containers*, NASA SP-106, 1966.

- Cho, J.R., Song, J.M. and Song, J.I. (1999), "Finite-element estimation of accurate added-masses in fluid-structure interaction problems," *Proc. 1st Int. Conf. Advances Struct. Engrg. Mechanics*, Seoul, Korea, 1641-1646.
- Cho, J.R., Lee, J.K., Song, J.M., Park, S.H. and Lee, J.N. (2000), "Free vibration analysis of aboveground LNG-storage tanks by the finite element method," *KSME International*, **14**(6), 633-644.
- Cho, J.R., Song, J.M. and Lee, J.K. (2001), "Finite element techniques for the free-vibration and seismic analysis of liquid-storage tanks," *Finite Elements in Analysis and Design*, **37**(6-7), 467-483.
- Cho, J.R. and Song, J.M. (2001), "Assessment of classical numerical models for the separate liquid-structure analysis," *J. of Sound and Vibration*, **239**(5), 995-1012.
- Conca, C., Osses, A. and Planchard, J. (1997), "Added mass and damping in fluid-structure interaction," *Comp. Meth. in Appl. Mech. and Eng.*, **146**, 387-405.
- Haroun, M.A. (1983), "Vibration studies and tests of liquid storage tanks," *Earthq. Eng. and Struct. Dyn.*, **11**, 179-206.
- Haroun, M.A. and Tayel, M.A. (1985), "Axisymmetrical vibrations of tanks-numerical," *J. Eng. Mech.*, **111**(3), 329-345.
- Housner, G.W. (1957), "Dynamic pressure on accelerated fluid containers," *Bull. Seism. Soc. Am.*, **47**, 15-35.
- Howe, M.S. (1998), *Acoustics of Fluid: Structure Interaction*, Cambridge University Press, New York.
- Mackerle, J. (1999), "Fluid-structure interaction problems, finite element and boundary element approaches-A bibliography (1995-1998)," *Finite Elements in Analysis and Design*, **31**, 231-240.
- Moiseev, N.N. and Rumyantsev, V.V. (1968), *Dynamic Stability of Bodies Containing Fluid*, Springer.
- Morand, H.J.-P. and Ohayon, R. (1995), *Fluid Structure Interaction: Applied Numerical Methods*, Wiley, New York.
- Rajasankar, J., Iyer, N.R. and Appa Rao, T.V.S.R. (1993), "A new 3-D finite element model to evaluate added mass for analysis of fluid-structure interaction problems," *Int. J. Numer. Meth. in Eng.*, **36**, 997-1012.
- Veletsos, A.S. (1963), "Seismic effects in flexible liquid storage tanks," *Proc. 5th World Conf. Earthquake Engrg.*, **1**, 367-390, Rome, Italy.
- Walker, S. (1980), "Boundary elements in fluid/structure interaction problems," *New Developments in Boundary Element Methods*, CML Publications, London.